Supporting Information for

High thermal conductivity states and enhanced figure of merit in aligned polymer thermoelectric materials

*Thibault Degousée, Viktoriia Untilova, Vishnu Vijayakumar, Xinzhao Xu, Yiwei Sun, Matteo Palma, Martin Brinkmann, Laure Biniek, Oliver Fenwick**

Dr. T. Degousée, Dr. Y. Sun, Dr. O. Fenwick
School of Engineering and Materials Science, Queen Mary University of London, Mile End Road, London E1 4NS, United Kingdom.
Email: o.fenwick@qmul.ac.uk

Dr. V. Untilova, Dr. V. Vijayakumar, Dr. L. Biniek, Dr. Martin Brinkmann
Université de Strasbourg, CNRS, ICS UPR 22, F-67000 Strasbourg, France.
Email: martin.brinkmann@ics-cnrs.unistra.fr; laure.biniek@ics-cnrs.unistra.fr

X. Xu, Dr. M. Palma
Department of Chemistry, Queen Mary University of London, Mile End Road, London E1 4NS, United Kingdom.
Email: m.palma@qmul.ac.uk

1. The 3ω method

The pre-patterned measurement chips (Linseis Messgeräte GmbH) are made of silicon with a top surface of 100 nm of silicon nitride. The substrate has been etched away in two locations to form two rectangular and free-standing membranes of silicon nitride whose thickness is 100 nm. The first membrane has an area of 4 x 0.4 mm^2 which we refer to as the "large" membrane. The second membrane has an area of 4 x 0.25 mm^2 which we refer to as the "small" membrane. Platinum rims where the membrane meets the substrate act as a heat sink, while thin wires of platinum (~100 nm thick, < 5µm wide) deposited on the membranes act as thermometer and heater. A passivation layer of 30 nm aluminium oxide sits on top of the SiN and Pt wires to prevent any electrical short-circuit during the measurement. More information on the design and characterization of the pre-patterned chips can be found elsewhere.[1-3] By applying an alternating current at a frequency ω to a thin film heater, its temperature oscillates at a frequency 2ω. This oscillation in temperature is accompanied by an oscillation in the resistance of the heater at the same frequency (2ω). The change in resistance introduces a component in the read-out voltage across the heater that is modulated at a frequency 3ω ($V_{3\omega}$). The amplitude of $V_{3\omega}$ can then be analysed by solving heat diffusion equations on the membrane: [1]

$$|V_{3\omega}| = \frac{\beta R_o^2 I_0^3}{4K_p \sqrt{1 + \omega^2 (4\tau^2 + \frac{w^4}{24D^2} + \frac{\tau w^2}{3D}}}$$

Equation (S1)

where β is the temperature coefficient of resistance of the thin film heater, R_0 the resistance of the unloaded heater, l and w are the length and width of the membrane, $K_p = 2\lambda t l/w$ with λt the thermal conductance of the entire system (membrane + sample), τ the thermal relaxation time defined by $\tau = C/K_p$ with C the heat capacity of the membrane, D is the diffusivity of the entire setup. At low frequency, the 3ω measurement is performed at nearly steady-state conditions which simplifies Equation S1 to:

$$|V_{3\omega}| = \frac{\beta R_0^2 I_0^3}{4K_p}$$

Equation (S2)

As the thermal conductance of the empty membrane is known from a blank chip measurement, the thermal conductivity of the sample λ_s can be obtained if its thickness t_s is known:

$$\lambda_s = \frac{\lambda t - \lambda_m t_m}{t_s}$$

Equation (S3)

Where λ and λ_m are the thermal conductivity of the entire setup and the membrane, respectively.

2. Transfer of the films to the TFA measurement chip

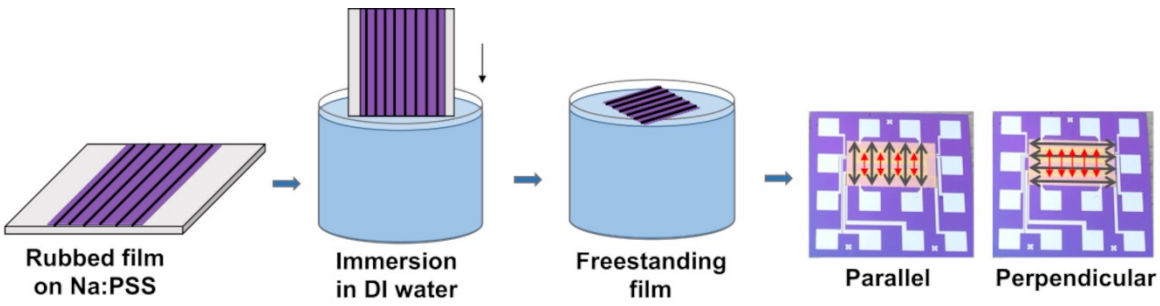

Figure S1 The P3HT (doped) films are immersed vertically in deionized water to dissolve the Na:PSS layer. The freestanding film the then transfer to the TFA measurement chip with the polymer chains parallel or perpendicular to the heat flux.

3. Film misalignment on test chips

Once the 3ω measurements had been performed, the chips were inspected by optical microscopy to exclude samples with cracks, defects, discontinuities in the film or folds due to transfer (example in Figure S1a). We used a two-dimensional Fast Fourier Transform (2D-FFT) on optical microscope images of successfully transferred samples to extract the angle between the polymer chains and the heater on the membranes (Figure S1b). As the length of the heater is much longer than its width, it is assumed to be 1D and its filtered signal is always a straight line. On the other hand, the filtered signal

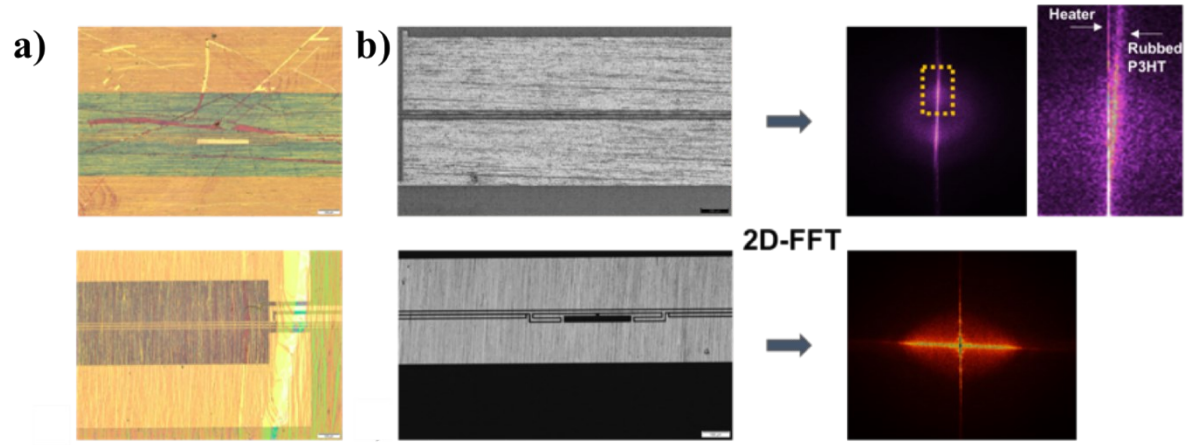

of the aligned polymer chains appears either perpendicular or parallel to the heater signal when the thermal conductivity is measured parallel or perpendicular to the chains, respectively (Figure S1b). The angle between the polymer signal and the heater signal in the 2D-FFT is used to calculate the misalignment angle. This method is direct and does not require perfectly horizontal optical images as the relative angle between the chains and the heater is extracted.

Figure S2 (a) Optical microscope image of rejected P3HT films. Top: sample presenting folds and cracks, the polymer chains are perpendicular to the heat flux. Bottom: sample presenting discontinuities in the film, the polymer chains are parallel to the heat flux. (b) Optical microscope images of successfully transferred samples with the polymer chains normal to (top) or parallel to (bottom) the heat flux. The misalignment angle between the polymer chains and the heater is extracted after filtering with a 2D-Fast Fourier Transform (2D-FFT). The misalignment angles presented here are 1.6° (top) and 3.8° (bottom).

4. Anisotropy in thermal conductivity

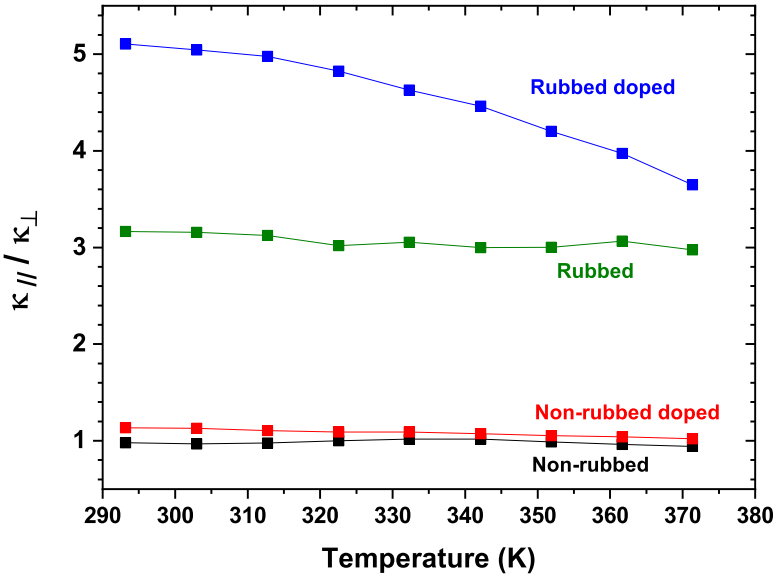

Figure S3 Anisotropy in thermal conductivity for the four films studied. $\kappa_{//}$ and $\kappa_{\perp}$ are the thermal conductivity parallel and perpendicular to the chain alignment directions respectively.

5. Nanoscale morphology of the rubbed (doped) films

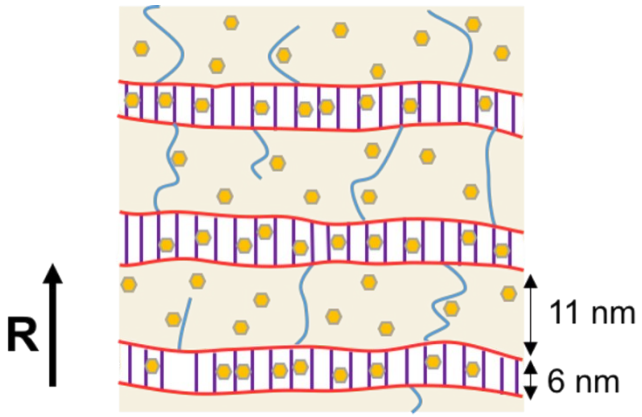

Figure S4 Schematic of the semi-crystalline morphology of the 171°C rubbed and doped films. The semi-crystalline morphology adopted after rubbing corresponds to an alternation of crystalline domains

(red/purple) separated by amorphous domains (pale yellow).[4] The yellow dots represent the dopant F_4TCNQ and the blue lines the possible tie-chains connecting the crystalline domains.

6. AFM and Quantitative Nanoscale Mechanical characterization (QNM)

Non-rubbed non-doped

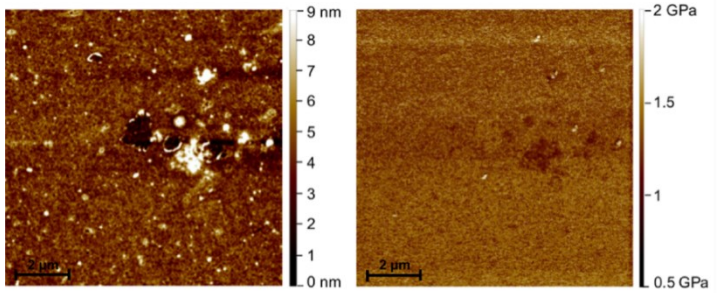

Non-rubbed doped

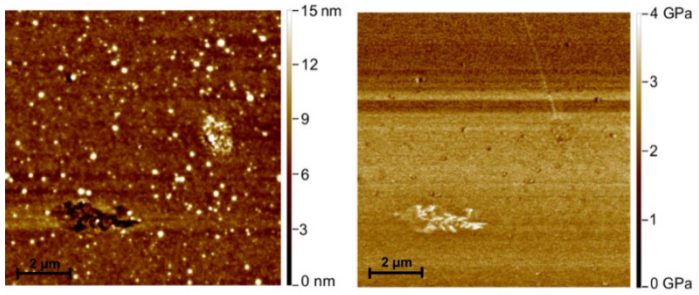

Rubbed non-doped

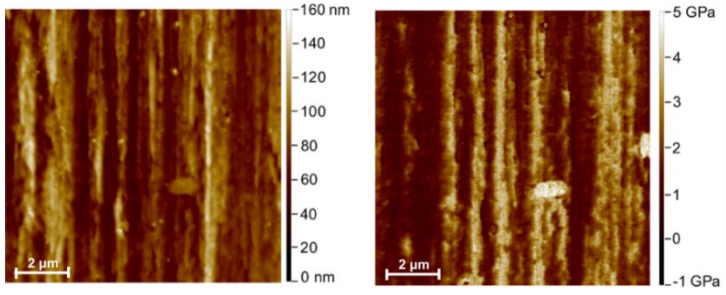

Rubbed doped

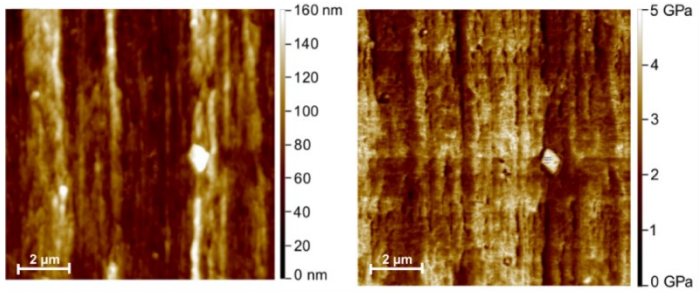

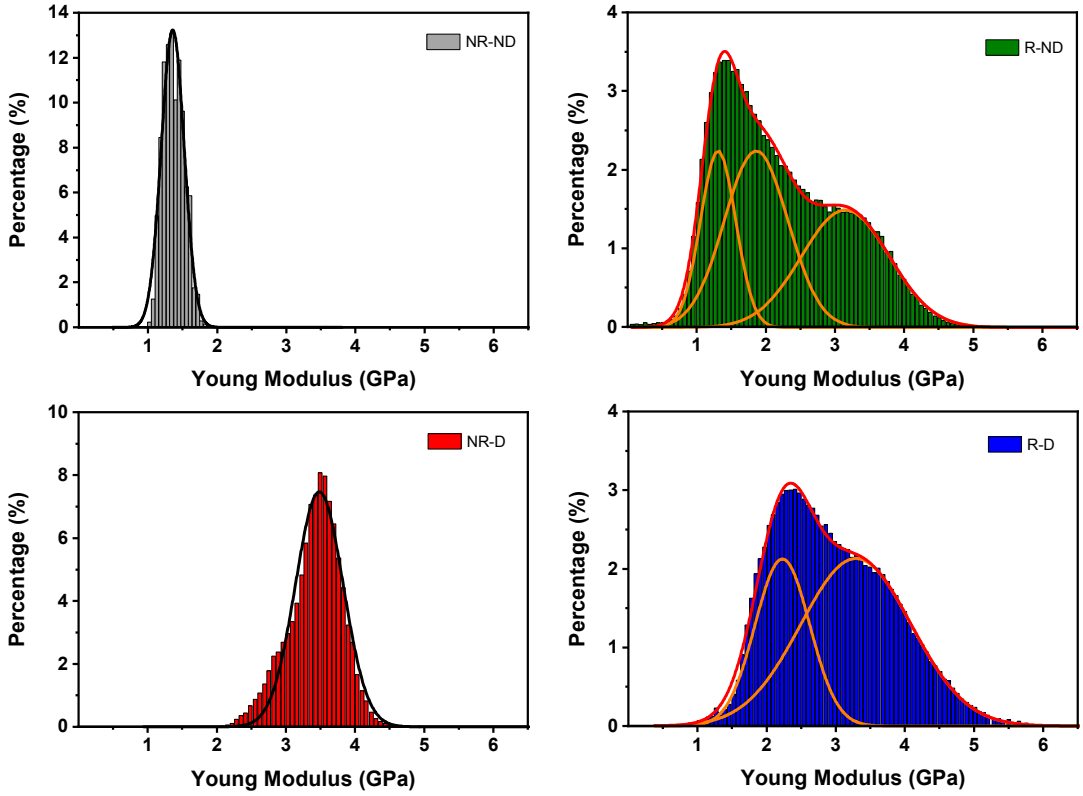

Figure S5 Atomic force microscopy images of isotropic (doped) and high-temperature rubbed (doped) films. Pictures on the left are the topographical images of the films (acquired in semi-contact tapping mode) and pictures on the right show the modulus extracted from QNM characterisations in Peak Force mode. The pictures size is 10 µm x 10 µm and the scale bar is 2 µm.

Figure S6 Young modulus of the isotropic (doped) and high-temperature rubbed (doped) films. NR-ND: non-rubbed non-doped, R-ND: rubbed non-doped, NR-D: non-rubbed doped, R-D: rubbed doped. The black and red lines correspond to a Gaussian fit of the Young modulus distribution. The distribution of the high-temperature rubbed films is split to represent the two regions of the rubbed films.

The distributions of the Young's modulus were fitted using a sum of multiple Gaussian peaks:

$$y = y_0 + \frac{A_i}{w_i\sqrt{\frac{\pi}{2}}} exp^{\left(-\left(\frac{x - xc_i}{2w_i}\right)^2\right)}$$

Where y_0 is the offset, A_i, w_i and xc_i are the amplitude, width and peak centre of each peaks, respectively.

7. Raman spectroscopy

As stated in the main text, we used an excitation wavelength of 785 nm, resonant with the doped species. The raw spectra along the deposition direction of the films excited at 785 nm are presented in Figure S7. The baseline of each measurement is subtracted using a spline function with eight anchor points (black squares in Figure S7). The same baseline subtraction is performed on the spectra acquired perpendicular to the deposition direction (not shown).

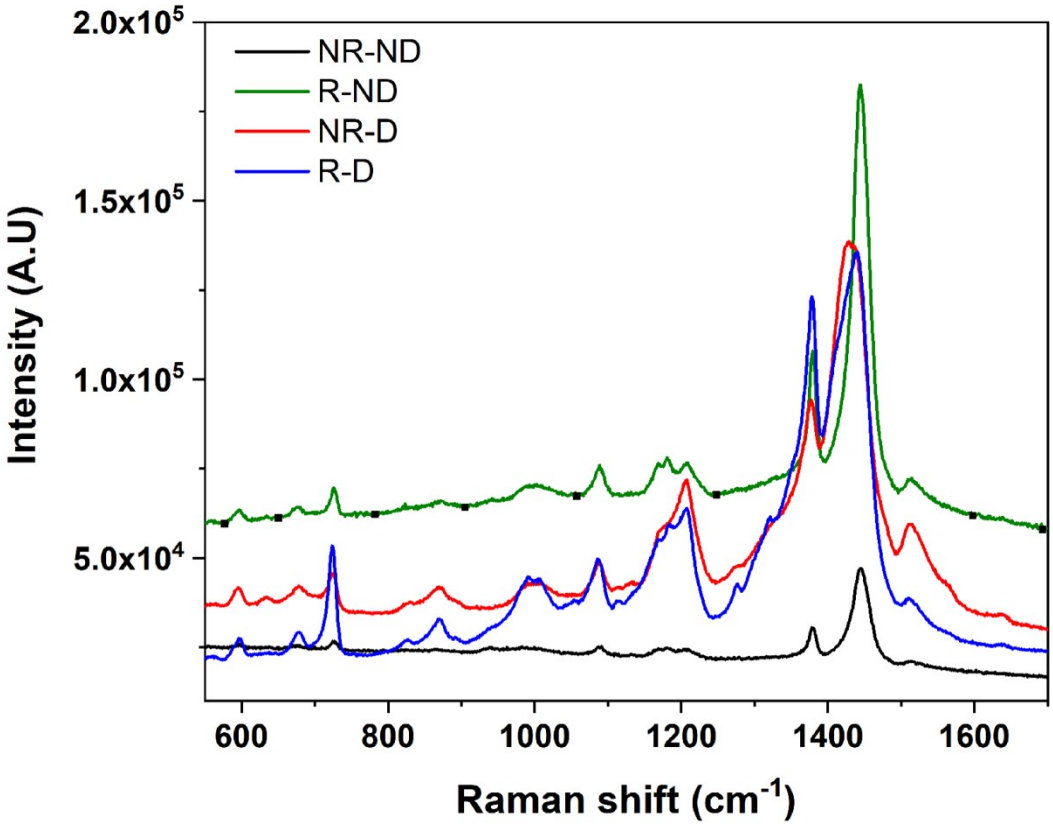

Figure S7 Raw Raman spectra along the deposition direction of isotropic P3HT (NR-ND), rubbed P3HT (R-ND) and their doped analogues (NR-D and R-D).

For the sake of comparison, all measurements have been normalized to the C=C ring breathing mode (Figure S8).

Prior to doping, the Raman spectra of NR-ND along and perpendicular to the doctor-blade deposition are identical (Figure S8 b). The vibration modes in the range 550-1250 cm^{-1} are listed in Figure S8 b accordingly to previous works on polythiophenes.[5-10] These vibration modes are also observed in the rubbed non-doped films, which present minimal difference between parallel and perpendicular directions (Figure S8 c).

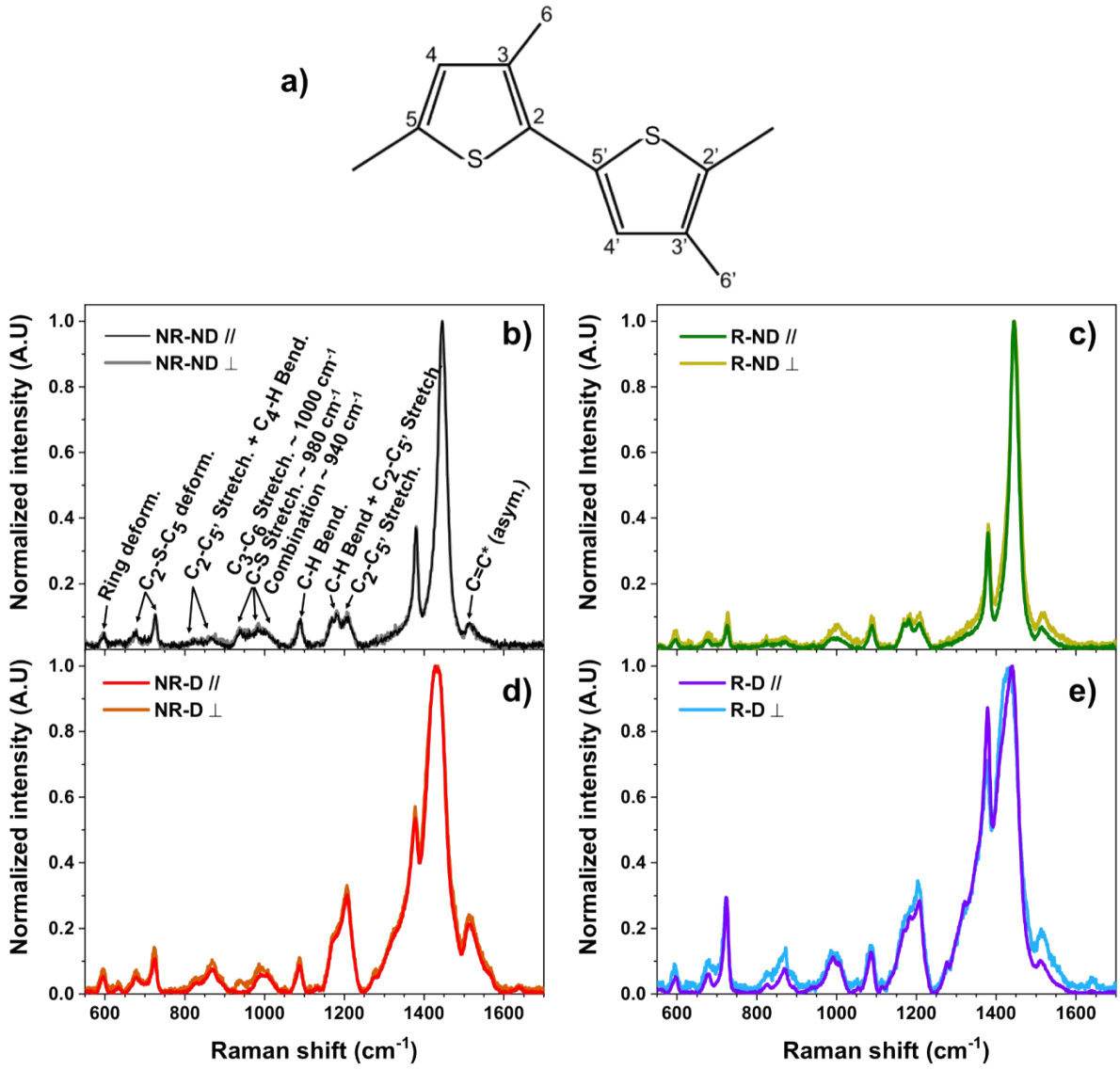

Figure S8 a) Schematic of P3HT with the corresponding carbon atoms labelled as in the normalized Raman spectra; Raman spectroscopy in the range 550-1700 cm^{-1} for b) isotropic non-doped (NR-ND), c) rubbed non-doped (R-ND), d) isotropic doped (NR-D) and e) rubbed doped (R-D) P3HT films. The parallel and perpendicular directions are relative to the deposition direction.

Upon immersion in F4TCNQ, the Raman spectrum of isotropic doped P3HT (NR-D) changes slightly, but there is still no difference in the features between seen parallel and perpendicular to the doctor-blade direction, consistent with the small anisotropy observed in the thermal conductivity measurement. Doping promotes the C_4-H bend + C_2-$C_{5'}$ stretching (800-900 cm^{-1}), the C_2-$C_{5'}$ stretching mode (~1205 cm^{-1}), and the combination modes C-H bend + C_2-$C_{5'}$ stretching (~1170 cm^{-1}). The normalized intensity of the C_2-S-C_5 deformation at ~724 cm^{-1} increases from 0.10 prior to doping to 0.11 (parallel) and 0.14 (perpendicular) after doping. For the rubbed doped films, the Raman spectra in the range 550-1250 cm^{-1} are similar in directions parallel and perpendicular to the rubbing direction (Figure S8 e). Doping also

promotes the vibrational modes around 800-900 cm^{-1} and 1170-1205 cm^{-1} for the rubbed films. However, the normalized intensity of the C_2-S-C_5 deformation triples from 0.10 to 0.30 upon doping of the rubbed films, both parallel and perpendicular to the rubbing direction. An increase of the intensity of vibration modes at 1170-1205 cm^{-1} and of the C_2-S-C_5 deformation are signatures of quinoid transition caused by polaron formation.[8, 11]

However, the most significant changes occur in the range 1250-1700 cm^{-1} (Figure S9) which is where the rest of the discussion will focus.

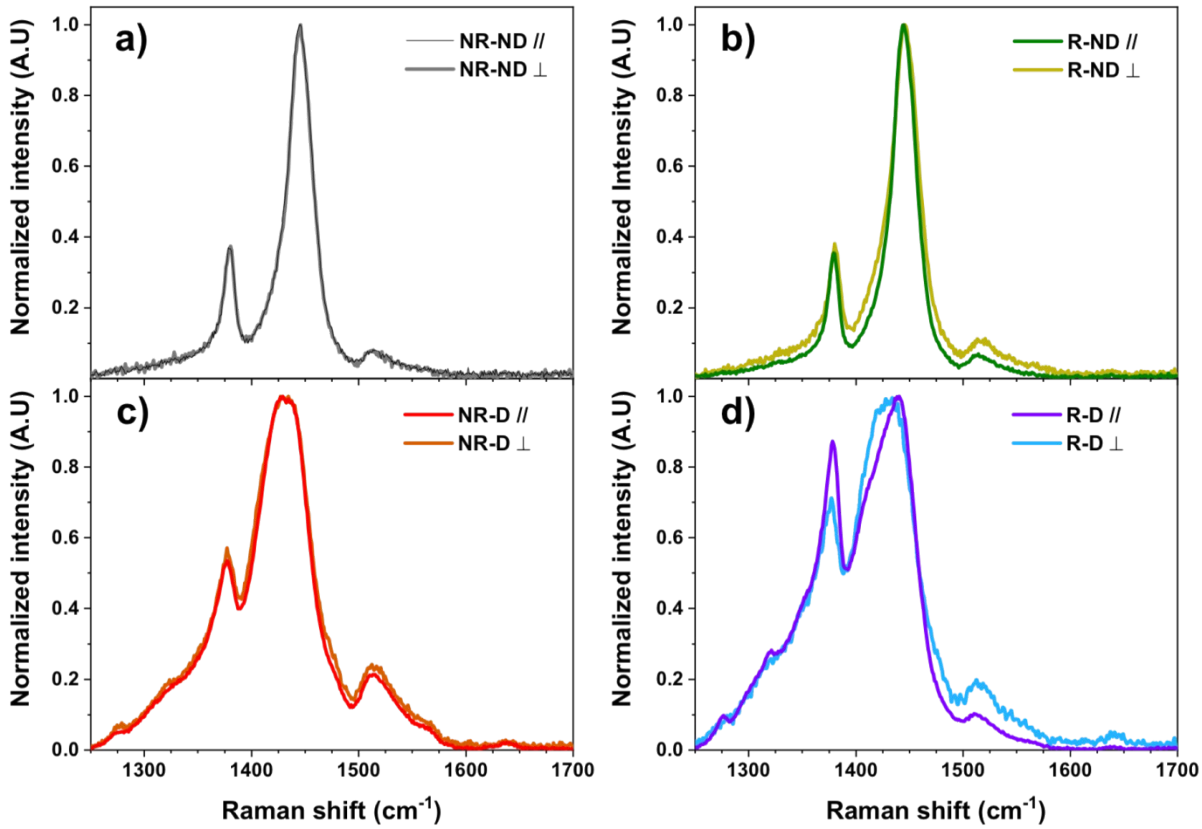

Figure S9 Raman spectroscopy in the range 1250-1700 cm^{-1} for a) isotropic non-doped (NR-ND), b) rubbed non-doped (R-ND), c) isotropic doped (NR-D) and e) rubbed doped (R-D) P3HT films. The parallel and perpendicular directions are relative to the deposition direction.

Prior to doping, the Raman line shape of isotropic and rubbed films are comparable, and there is no difference whether assessed parallel or perpendicular (Figure S9 a, b). We observe a peak at ~1380 cm^{-1} which is attributed to C_3-C_4 stretching, the main C=C stretching (ring breathing) at 1445 cm^{-1}, and the C=C* asymmetric stretching at ~ 1510 cm^{-1}.

Upon doping of the isotropic films (Figure S9 c), new Raman modes are seen in the region 1250-1380 cm^{-1}.[5-8] The C_3-C_4 stretching peak position shifts to 1377 cm^{-1} and its normalized intensity increases from 0.37 to 0.56 as expected upon doping. This increase of the C_3-C_4 stretching intensity is a marker

of the quinoid transition upon formation of polarons.[7, 11] The main peak (C=C stretching) broadens and is shifted to ~1431 cm^{-1}, while the normalized intensity of the C=C* asymmetric stretching nearly triples (0.08 to 0.23).

For the rubbed doped films, the normalized intensity of the C_3-C_4 stretching is nearly as intense as the main vibration peak, reaching 0.87 along the rubbing direction and 0.71 perpendicular to it (Figure S9 d). This higher ratio of the C-C stretching over the C=C stretching indicates greater planar configuration and translates to more efficient electrical charge transport. Furthermore, the line shapes parallel or perpendicular to the rubbing direction are different. The line shape perpendicular is comparable to isotropic doped P3HT films, with a broadening and shifting of the C=C stretching to 1433 cm^{-1} and a C=C* stretching that is twice as intense (Figure S9 d). Looking parallel to the rubbing direction (Figure S9 d), the peak position of the C=C stretching is 1440 cm^{-1} and a shoulder around 1415 cm^{-1} can be seen. The C=C* asymmetric stretching is less affected by doping as it only increases to 0.11 (0.07 prior to doping). Furthermore, the right tail of the C=C stretching (~1470 cm^{-1}) associated with P3HT disordered C=C contributions[12] is not as significant when assessed parallel to the rubbing direction as the perpendicular results. This suggests that there is more order parallel to the rubbing direction than perpendicular to it.

Deconvolution of the Raman spectrum

Recently, Nightingale *et al.* showed that deconvolution of in-situ Raman measurements during electrochemical oxidation gives a deeper view on the morphology of P3HT thin films.[5] We used a similar approach to look at the effect of high-temperature rubbing and doping on our P3HT films. The main C=C stretching was composed of four vibration modes: C=C charged disordered (~1405 cm^{-1}), C=C charged ordered (~1420 cm^{-1}), C=C neutral ordered (~1445 cm^{-1}) and C=C neutral disordered (~1470 cm^{-1}). Raman spectroscopy probes the vibrational modes of molecules and so "ordered" and "disordered" refers to order at the level of the polymer chain rather than regions of the film. Therefore an "ordered" mode would relate to a polymer segment where there is a long conjugation length containing a large number of thiophene units without kinks or twists. DFT simulations[13] have been used to simulate shifts in the Raman spectra related to length of conjugated segments and their planarity, with a good match to experimental data for regioregular (relatively ordered) and regiorandom (relatively amorphous) P3HT films. The C=C symmetric stretch (at ~1450 cm^{-1}) shifts to shorter wavelength and narrows for longer conjugation length and greater planarity. Although "order" is defined at the level of an individual chain, crystalline domains in polymer films will tend to contain a greater proportion of ordered segments with long conjugation length, whereas amorphous regions will contain segments with a lower average conjugation length.

When polarons are considered, the definitions of ordered and disordered chain segments are split into neutral and charged. Neutral ordered and neutral disordered chain segments are as defined above. Charged ordered and charged disordered chain segments are polaron containing chain segments that were ordered and disordered, respectively, in their neutral state. The difference in polaron structure between the two cases comes from the effective conjugation length which is larger on the initial "ordered" segments. On these ordered segments there is a relatively small conformational change to accommodate the polaron, but there are larger changes in bond length when a polaron forms on shorter segments causing greater shifts in the Raman signal. It is therefore possible to distinguish polarons on ordered (long conjugation length) and disordered (short conjugation length) chain segments.

In their work, Nightingale *et al.* fixed the peak position of all modes excepted for the C=C charged disordered to look at the effect of doping on this mode.[5] They also fixed the FWHM of all modes except for the C=C charged ordered mode to look at new charged ordered phases induced by doping. Owing to our results for the isotropic doped films (high thermal conductivity and Young modulus despite a moderate increase of the electrical conductivity) and the distinct Raman line shapes, we constrained the peak positions and FWHM of the peaks instead of fixing them. The peak position of the four modes were allowed a shift of ± 10 cm^{-1} from their original position. The FWHM were constrained between 1 cm^{-1} and 50 cm^{-1} excepted for the C=C charged disordered vibration mode constrained between 1 cm^{-1} and 20 cm^{-1}, in line with the literature.[5] The amplitude of the peak was unconstrained to look at the fraction of modes induced by high-temperature rubbing and doping. We defined five peaks induced by doping in the range 1250-1365 cm^{-1}. Peak positions were evaluated by looking at the Raman line shapes before applying the same constraints as for the four main vibration modes during the fitting procedure. The C_3-C_4 stretching at ~1380 cm^{-1} was left unconstrained. All the fitting procedures were stopped when $R^2 > 0.99$.

For the non-doped films, the deconvolutions are almost identical whether we look along or perpendicular to the deposition direction (Figure S10 a-d). The peak parameters of the four main vibrations modes, listed in Table S1, are in excellent agreement with the work of Nightingale *et al.* Using the integrated peak area, we plotted the proportion of each vibration mode to the total C=C ring breathing (Figure S10 e). For both type of films and in both directions, the C=C neutral ordered mode provides the main contribution (54-67 %) while the C=C neutral disordered mode represents 18-31%. We attribute the presence of charged vibration modes to doping upon air exposure.

Table S1: Peak parameters for the C=C charged (dis)ordered (C=C*) and C=C neutral (dis)ordered along and perpendicular to the deposition direction of non-doped films.

	NR-ND //				**R-ND //**			
	C=C* (disord.)	C=C* (ord.)	C=C (ord.)	C=C (disord.)	C=C* (disord.)	C=C* (ord.)	C=C (ord.)	C=C (disord.)
Position (cm^{-1})	-	1415	1445	1460	-	1417	1445	1460
FWHM (cm^{-1})	-	30	25	42	-	30	25	39
Amplitude	0.0	0.20	0.85	0.16	0.0	0.20	0.87	0.15
	NR-ND □				**R-ND □**			
Position (cm^{-1})	-	1417	1445	1462	-	1417	1446	1471
FWHM (cm^{-1})	-	30	25	39	-	30	27	30
Amplitude	0.0	0.22	0.86	0.15	0.0	0.27	0.93	0.14

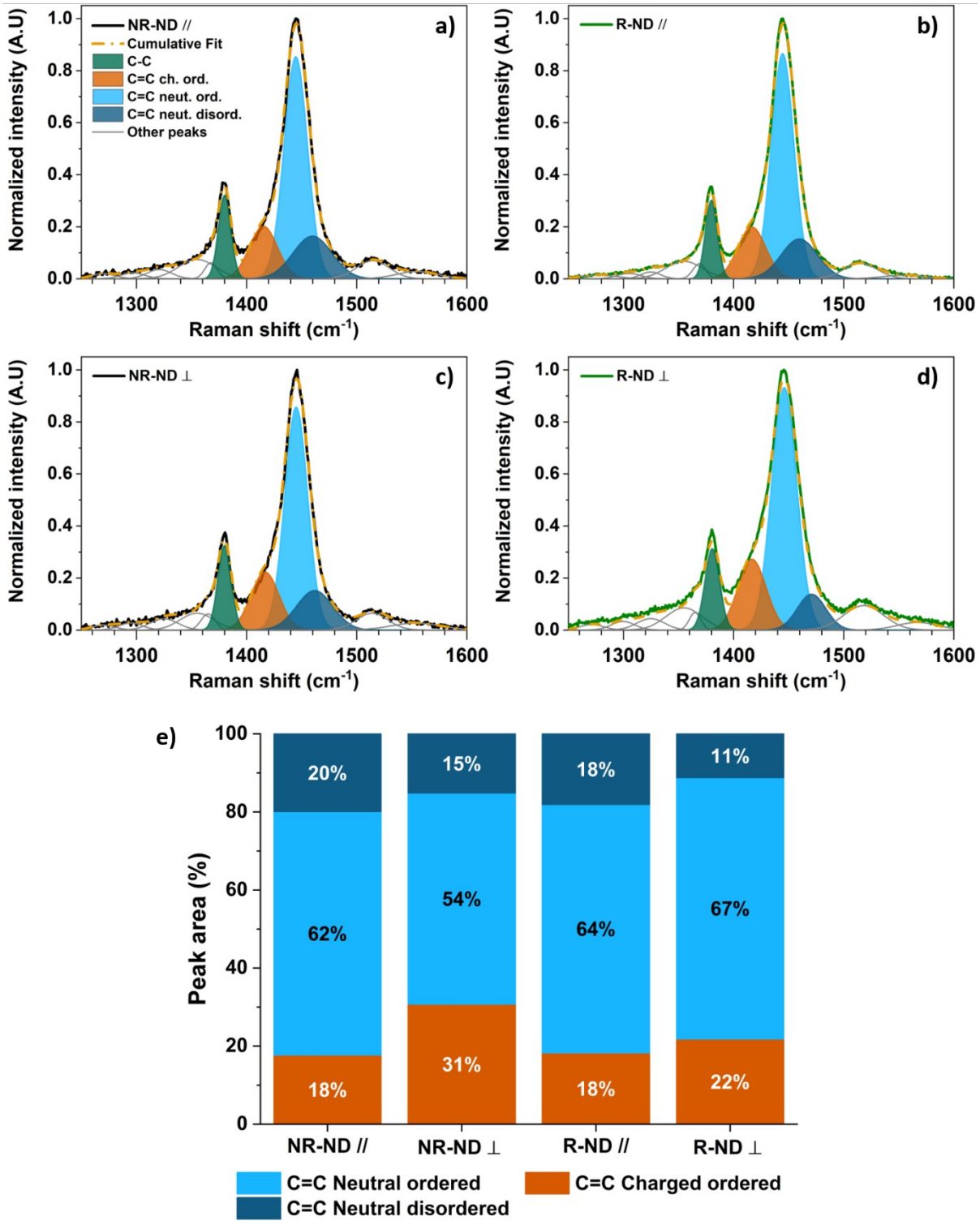

Figure S10 Deconvolution of Raman spectroscopy in the range 1250-1600 cm^{-1} for isotropic non-doped (NR-ND) a) parallel and c) perpendicular to the doctor-blade direction; rubbed non-doped (R-ND) b) parallel and d) perpendicular to the rubbing direction; and e) total integrated peak area of the four vibration modes of the C=C ring breathing.

We then look at the deconvolution of the doped films, where it is clear that isotropic doped P3HT and rubbed doped perpendicular are comparable (Figure S11 a, c, d). For these samples, the C=C neutral ordered vibration mode remains the main contribution to the C=C ring breathing upon doping, representing 52-57% of the total peak area (Figure S11 a, c, d, e). However, its peak position shifts to ~1440 cm^{-1} and its FWHM increases to 34-38 cm^{-1} (Table S2). This broadening implies that, in the solid state, more conformations of neutral ordered P3HT segments participate in the C=C neutral ordered vibration mode. Furthermore, according to the effective conjugation coordinate model (ECC), the decrease to a lower wavenumber could be explained by a more planar conformation of the neutral ordered segments upon doping.[13] Moreover, doping has a strong impact on the C=C neutral disordered vibration mode, whose peak position in the non-rubbed films is blue-shifted by ~13 cm^{-1} to ~1474 cm^{-1} and its FWHM decreases by ~15 cm^{-1} (Table S2). As a result, the proportion of the peak area decreases by a factor of ~2 as compared to the non-doped samples, representing 7-11% of the C=C ring breathing (Figure S11 e). The majority of the charged species formed upon doping appear to be in an ordered configuration. The C=C charged disordered mode at ~1398 cm^{-1} represents ~10% of the total peak area proportion in these films while the C=C charged ordered mode at ~1415 cm^{-1} represents ~25% (Figure S11).

Rubbed doped films assessed parallel to the rubbing direction (Figure S11 b) are strikingly different from all the other doped films. First of all, the C=C neutral ordered vibration mode does not shift or broaden significantly; only its amplitude decreases as a consequence of doping. This vibration mode represents 21% of the total peak area of the C=C ring breathing (Figure S11 e). Secondly, assessment along the rubbing direction shows a mostly charged and ordered film, with the C=C charged ordered mode at 1421 cm^{-1} representing 65% of the total peak area proportion, whilst the C=C charged disordered at 1405 cm^{-1} represents only 3%. The impact of doping on the C=C neutral disordered peak is less pronounced than in other doped films, with a blue shift of 7 cm^{-1} and no broadening.

Table S2: Peak parameters for the C=C charged (dis)ordered (C=C*) and C=C neutral (dis)ordered, parallel and perpendicular to the deposition direction of doped films.

	NR-D //				**R-D //**			
	C=C* (disord.)	C=C* (ord.)	C=C (ord.)	C=C (disord.)	C=C* (disord.)	C=C* (ord.)	C=C (ord.)	C=C (disord.)
Position (cm^{-1})	1398	1417	1440	1474	1397	1421	1444	1467
FWHM (cm^{-1})	20	26	34	27	20	50	27	42
Amplitude	0.32	0.61	0.89	0.18	0.09	0.76	0.47	0.15
	NR-D □				**R-D □**			
Position (cm^{-1})	1398	1415	1440	1474	1398	1415	1439	1473
FWHM (cm^{-1})	20	28	37	23	20	25	38	26
Amplitude	0.27	0.58	0.90	0.18	0.37	0.55	0.91	0.18

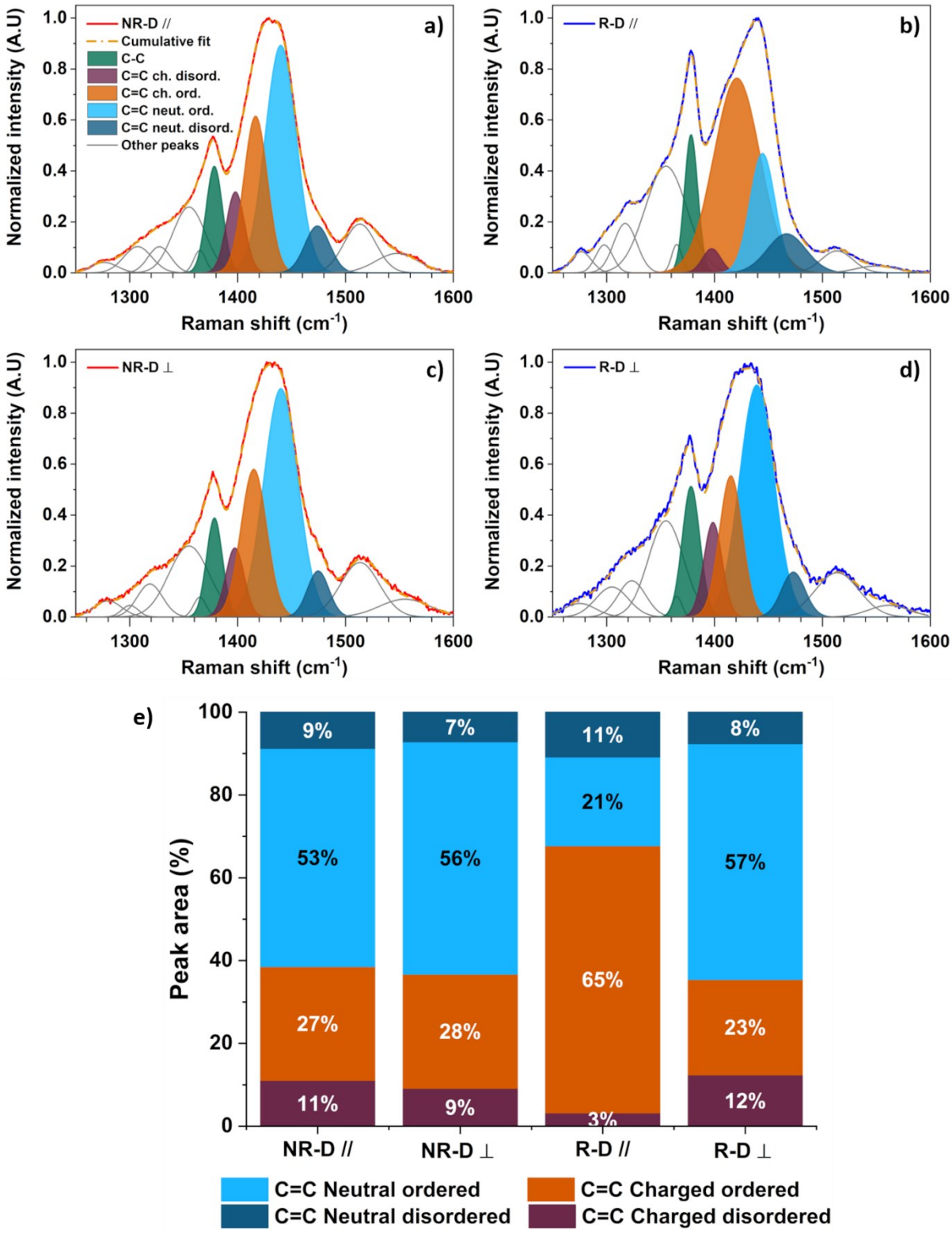

Figure S11 Deconvolution of Raman spectroscopy in the range 1250-1600 cm^{-1} for isotropic doped (NR-D) a) parallel and c) perpendicular to the doctor-blade direction; rubbed doped (R-ND) b) parallel and d) perpendicular to the rubbing direction; and e) total integrated peak area of the four vibration modes of the C=C ring breathing.

References

1. V. Linseis, F. Völklein, H. Reith, K. Nielsch and P. Woias, *Rev. Sci. Instrum.*, 2018, **89**, 015110.
2. V. Linseis, F. Völklein, H. Reith, P. Woias and K. Nielsch, *J. Mater. Res.*, 2016, **31**, 3196-3204.
3. V. Linseis, F. Völklein, H. Reith, P. Woias and K. Nielsch, *J. Electron. Mater.*, 2018, **47**, 3203-3209.
4. A. Hamidi-Sakr, Biniek, L., Fall, S. and Brinkmann, M., *Adv. Func. Mater.*, 2015, **26**, 408-420.
5. J. Nightingale, J. Wade, D. Moia, J. Nelson and J.-S. Kim, *J. Phys. Chem. C*, 2018, **122**, 29129-29140.
6. G. Louarn, J. Y. Mévellec, S. Lefrant, J. P. Buisson, D. Fichou and M. P. Teulade-Fichou, *Synth. Met.*, 1995, **69**, 351-352.
7. G. Louarn, M. Trznadel, J. P. Buisson, J. Laska, A. Pron, M. Lapkowski and S. Lefrant, *J. Phys. Chem. A*, 1996, **100**, 12532-12539.
8. S. Lefrant, I. Baltog, M. Lamy de la Chapelle, M. Baibarac, G. Louarn, C. Journet and P. Bernier, *Synth. Met.*, 1999, **100**, 13-27.
9. B. Sainbileg, Y.-B. Lan, J.-K. Wang and M. Hayashi, *J. Phys. Chem. C*, 2018, **122**, 4224-4231.
10. T. J. Magnanelli and A. E. Bragg, *J. Phys. Chem. Lett.*, 2015, **6**, 438-445.
11. J. Yamamoto and Y. Furukawa, *J. Phys. Chem. B*, 2015, **119**, 4788-4794.
12. Y. Gao and J. K. Grey, *J. Am. Chem. Soc.*, 2009, **131**, 9654-9662.
13. W. C. Tsoi, D. T. James, J. S. Kim, P. G. Nicholson, C. E. Murphy, D. D. C. Bradley, J. Nelson and J.-S. Kim, *J. Am. Chem. Soc.*, 2011, **133**, 9834-9843.